








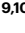


A short-term, high-caloric diet has prolonged effects on brain insulin action in men

Received: 15 April 2024

Accepted: 30 January 2025

Published online: 21 February 2025

 Check for updates

Stephanie Kullmann ^{1,2,3}✉, Lore Wagner ^{1,2}, Robert Hauffe^{2,4,5},
Anne Kühnel ⁶, Leontine Sandforth^{1,2,3}, Ralf Veit ^{1,2}, Corinna Dannecker^{1,2},
Jürgen Machann ^{1,2,7}, Andreas Fritsche^{1,2,3}, Nibert Stefan^{1,2,3},
Hubert Preissl ^{1,2,3}, Nils B. Kroemer ^{6,8}, Martin Heni ^{9,10},
André Kleinridders ^{2,4,5} & Andreas L. Birkenfeld ^{1,2,3}

Brain insulin responsiveness is linked to long-term weight gain and unhealthy body fat distribution. Here we show that short-term overeating with calorie-rich sweet and fatty foods triggers liver fat accumulation and disrupted brain insulin action that outlasted the time-frame of its consumption in healthy weight men. Hence, brain response to insulin can adapt to short-term changes in diet before weight gain and may facilitate the development of obesity and associated diseases.

Insulin resistance is a common feature of obesity and type 2 diabetes with detrimental effects in the periphery¹ and the central nervous system². In the healthy state, insulin acts in the brain in an anorexigenic fashion reducing appetite and food intake³, whereas in the insulin-resistant state, brain insulin action no longer properly regulates peripheral energy metabolism and feeding behaviour^{2,4,5}. Concurrently, people with aberrant insulin response have higher visceral adipose tissue mass and impaired peripheral metabolism^{6–8} and regain more fat mass after a lifestyle intervention⁷. Furthermore, findings from numerous studies suggest that the disruption of insulin responsiveness in the human brain promotes metabolic, psychiatric and neurodegenerative diseases^{4,9}. However, the developmental trajectory of brain insulin responsiveness in humans is currently unclear. To close this gap, we investigated the effect of a 5-day high-caloric diet (HCD) that included broadly available and commonly consumed, calorie-rich ultra-processed snacks in addition to the regular diet, compared with a regular diet on brain insulin action, body fat composition and peripheral insulin sensitivity. To study the brain-specific effects of insulin action, intranasal insulin (INI) application was used as a noninvasive method for the delivery of insulin to the brain in combination with

functional magnetic resonance imaging (fMRI). Our primary aim was to assess brain insulin activity before, directly after the HCD compared with a normal caloric diet and 1 week after the return to a regular diet. Previous experimental findings indicate sex differences in the response to INI affecting appetite, metabolism and memory function^{3,10}. Hence, we only evaluated brain insulin action in response to overeating in healthy weight male participants to investigate the temporal dynamics of brain insulin action in response to an unhealthy diet.

In a nonrandomized controlled design, a total of 29 male volunteers (age 19–27 years, body mass index (BMI) 19–25 kg m⁻²) enrolled to participate either in a 5-day HCD ($n = 18$) or a regular diet ($n = 11$; no additional calories) (Table 1). Participants completed three visits (baseline, follow-up 1 and follow-up 2) during an assessment period of approximately 3–4 weeks (see Fig. 1 for study design). Seventeen of the HCD group completed all three visits. The HCD group were instructed to increase their daily caloric intake by 1,500 kcal for five consecutive days with high-caloric ultra-processed snacks 5 days before follow-up 1 visit. Thereafter, HCD group participants resumed their regular diet for 7 days before follow-up 2. Eleven participants maintained their habitual diet throughout the study. The food diary showed that the HCD

¹Institute for Diabetes Research and Metabolic Diseases of the Helmholtz Center Munich at the University of Tübingen, Tübingen, Germany. ²German Center for Diabetes Research (DZD), Neuherberg, Germany. ³Department of Internal Medicine, Division of Diabetology, Endocrinology and Nephrology, Eberhard Karls University Tübingen, Tübingen, Germany. ⁴Institute of Nutritional Science, Department of Molecular and Experimental Nutritional Medicine, University of Potsdam, Nuthetal, Germany. ⁵German Institute of Human Nutrition, Junior Research Group Central Regulation of Metabolism, Nuthetal, Germany. ⁶Section of Medical Psychology, Department of Psychiatry and Psychotherapy, Faculty of Medicine, University of Bonn, Bonn, Germany. ⁷Section on Experimental Radiology, Department of Radiology, University Hospital Tübingen, Tübingen, Germany. ⁸Department of Psychiatry and Psychotherapy, Tübingen Center for Mental Health (TüCMH), University of Tübingen, Tübingen, Germany. ⁹Institute for Clinical Chemistry and Pathobiochemistry, Department for Diagnostic Laboratory Medicine, Eberhard Karls University Tübingen, Tübingen, Germany. ¹⁰Division of Endocrinology and Diabetology, Department of Internal Medicine I, University of Ulm, Ulm, Germany. ✉e-mail: stephanie.kullmann@med.uni-tuebingen.de

Table 1 | Participants' metabolic characteristics

	Control		HCD	
	Baseline	Follow-up 1	Baseline	Follow-up 1
Body composition				
Body weight (kg)	73.9±7.1	74.6±7.0	72.3±9.1	72.8±9.4
BMI (kg m ⁻²)	22.15±1.4	22.35±1.3	21.82±2.4	21.95±2.5
Waist-to-hip ratio	0.85±0.1	0.86±0.1	0.86±0.1	0.86±0.04
Total adipose tissue, MR-derived (l)	18.85±5.7	18.16±5.2	16.93±4.7	17.43±4.6
Subcutaneous adipose tissue, lower extremity, MR-derived (l)	8.74±2.5	8.40±2.3	8.04±2.2	8.28±2.1
Visceral adipose tissue, MR-derived (l)	1.60±0.7	1.63±0.6	1.70±0.87	1.69±0.9
Liver fat, ¹ H-MRS-derived (%) ^a	1.08±0.6	1.22±1.1	1.55±2.2	2.54±3.5
Metabolic parameters				
At follow-up 2: only fasting insulin, glucose, CRP and γ -glutamyl transferase were available				
	Baseline	Follow-up 1 Follow-up 2	Baseline	Follow-up 1 Follow-up 2
HbA1c (%)	5.16±0.2	5.15±0.2	5.08±0.3	5.09±0.2
HbA1c (mmol mol ⁻¹)	32.82±2.3	32.82±2.5	32.12±2.6	31.94±1.9
Matsuda insulin sensitivity index (oGTT-derived)	18.15±6.9	15.70±5.7	18.12±6.5	16.27±6.2
HOMA-IR	1.9±0.8	2.1±0.7 1.6±0.9	1.7±0.7	1.9±0.7 1.7±0.5
Fasting insulin (pmol l ⁻¹)	54.82±22.5	61.09±18.1 46.60±23.5	47.44±17.8	54.67±18.6 48.65±14.3
Fasting glucose (mmol l ⁻¹)	4.68±0.4	4.77±0.4 4.67±0.3	4.77±0.3	4.64±0.3 4.61±0.3
Fasting glucagon (pg ml ⁻¹)	84.18±6.3	85.82±7.3	85.78±5.8	83.5±5.7
Fasting triglycerides (mg dl ⁻¹)	69.18±23.1	68.36±29.1	65.61±22.2	73.11±33.1
IL-6-HS (pg ml ⁻¹)	1.08±0.70	0.96±0.62	1.01±0.92	0.84±0.43
CRP (mg l ⁻¹)	0.04±0.06	0.07±0.13	0.06±0.08	0.05±0.06 0.10±0.17
γ -Glutamyl transferase (U l ⁻¹)	21.00±6.6	19.82±7.3	21.39±15.7	19.94±13.1 20.24±15.9
Testosterone (nmol l ⁻¹)	17.49±4.2	17.51±4.5	19.18±7.1	19.08±5.2 18.76±5.4
Indirect calorimetry				
Resting energy expenditure (kcal)	2,115±219	2,166±216	2,195±260	2,155±275
Respiratory quotient	0.85±0.1	0.89±0.1	0.86±0.1	0.88±0.1

Data are presented as mean±s.d. ^aFor liver fat, we observed a significant group-by-visit interaction of $P=0.008$. MR, magnetic resonance; HbA1c, glycated haemoglobin; MRS, magnetic resonance spectroscopy. $n=29$.

group increased their daily total caloric intake on average by 1,200 kcal between the baseline and follow-up 1 visit ($P < 0.05$; Extended Data Table 1). No within-HCD group differences were observed between baseline and follow-up 2 visit ($P < 0.05$). Total caloric intake, including major macronutrient composition, did not differ between HCD and the control group at baseline and at the follow-up 2 study visit (no main effect of group or group-by-visit interaction; $P > 0.05$; Extended Data Table 1). There was a significant main effect of visit (baseline versus follow-up 2) for total caloric intake and all major macronutrient compositions ($P < 0.05$), with lower reported food intake at follow-up 2 compared with the baseline for both groups. State questionnaires on mood, desire to eat and food cravings showed no group differences across visits in the fasted state (Extended Data Table 2). Body weight and body composition did not differ between the groups and visits ($P > 0.05$; Table 1). However, liver fat content increased in the HCD

group (group-by-visit interaction, estimate of -0.11 , 95% CI -0.19 to -0.03 , $P = 0.008$; HCD group baseline versus HCD follow-up 1, estimate of -0.3744 , s.e. = 0.104 , d.f. = 30.4 , $t = 3.6$, $P = 0.005$; Extended Data Fig. 1), whereas it did not change in the control group ($P = 0.958$). No significant differences were identified for metabolic parameters ($P > 0.05$; Table 1), including peripheral insulin sensitivity based on the oral glucose tolerance test (oGTT)-derived Matsuda Index and the homeostasis model assessment insulin resistance (HOMA-IR), as well as inflammatory markers such as C-reactive protein (CRP), interleukin (IL)-6 (Table 1) and other cytokines (Extended Data Table 3).

The primary aim of the study was to assess insulin-induced brain activity before (baseline), directly after the HCD (follow-up 1) and 1 week after a normal caloric diet was resumed (follow-up 2) compared with a control group maintaining their regular diet. The absolute change of cerebral blood flow (CBF) was used as a proxy for neural

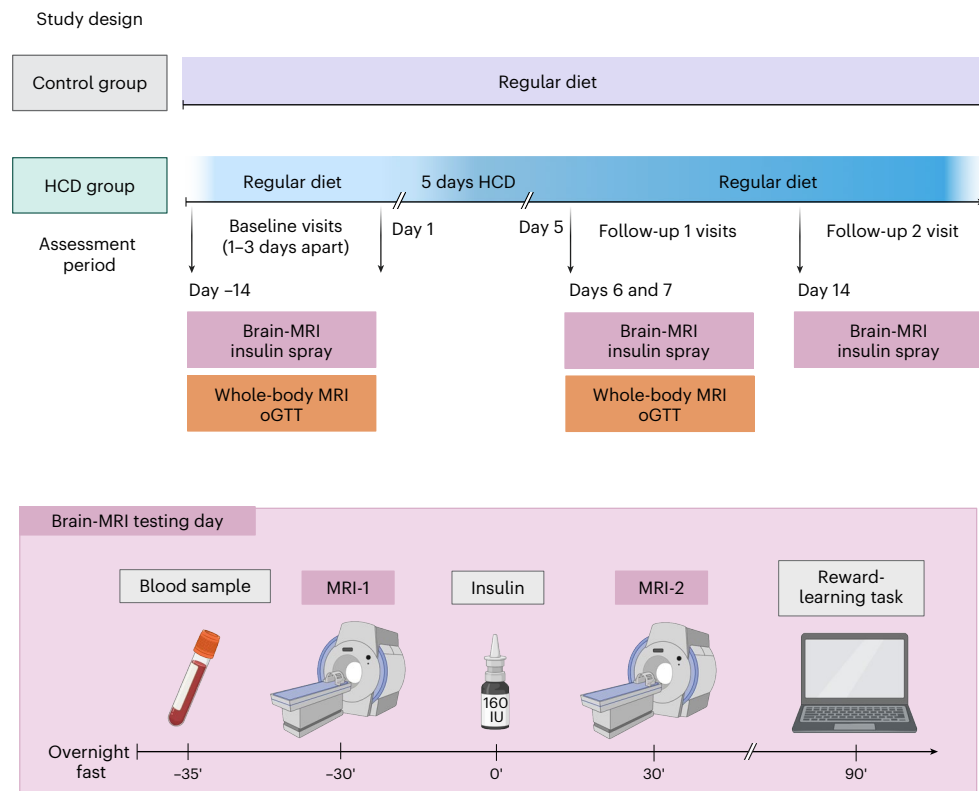


Fig. 1 | Schematic overview of the study design. After initial screening, healthy weight male participants underwent two baseline assessment days after an overnight fast at -08:00. On the brain MRI testing day, diffusion-weighted imaging and CBF responses to 160 IU INI were acquired to investigate white matter integrity and brain insulin action ($\Delta\text{CBF} = \text{CBF MRI-2} - \text{CBF MRI-1}$), respectively, followed by a reward-learning task. On a separate testing day (1–3 days apart), whole-body MRI for measurement of body fat mass and distribution and oGTTs for measurement of peripheral insulin sensitivity were performed. Afterwards, 18 participants were instructed to increase their daily caloric

intake by 1,500 kcal for five consecutive days with high-caloric snacks. Eleven participants maintained their regular diet. Both testing days were repeated immediately after the 5-day HCD or regular diet period at follow-up 1. At follow-up 2, the brain MRI testing day was repeated 7 days after resuming a regular diet. Eating behaviour questionnaires were acquired during all testing days. Between visits, participants recorded their food intake and daily step activity. The timing of the follow-up visits was adapted to the first day of the HCD recording. Figure created in [BioRender](#)⁵⁰.

activity. We analysed the difference in brain insulin activity between the HCD and control groups at follow-up 1 and follow-up 2, adjusted for the individual baseline measurement (Fig. 2a). The HCD group had significantly higher insulin activity in parts of the right insular cortex, left rolandic operculum and right midbrain/pons (Fig. 2b) at follow-up 1 adjusted for baseline compared with the control group ($P_{\text{FWE}} < 0.05$, whole-brain corrected, where FWE indicates family wise error; Extended Data Table 4). At the second follow-up, 7 days after resuming the regular diet, the HCD group showed significantly lower brain insulin activity in the right hippocampus and bilateral fusiform gyrus compared with the control group (Fig. 2c; $P_{\text{FWE}} < 0.05$, whole-brain corrected; Extended Data Table 4). No differences were observed in hypothalamic response to insulin between the HCD and control groups at both follow-up time points ($P > 0.05$). At the baseline visit, no group differences were observed for the absolute change of CBF from before to after INI ($P_{\text{FWE}} > 0.05$). Independent of INI, we observed no differences between the HCD and the control group in regional CBF or global CBF (CBF before nasal spray application HCD versus controls; $P_{\text{FWE}} > 0.05$).

We further evaluated whether the HCD alters reward and punishment sensitivity. Compared with the control group, the HCD reduced reward sensitivity ($t(27) = -3.6$, $P_{\text{boot}} < 0.001$, where boot indicates bootstrapping) and increased punishment sensitivity ($t(27) = 2.6$, $P_{\text{boot}} = 0.002$) at follow-up 1 (Extended Data Fig. 2). Notably, this pattern was still evident at follow-up 2, although the effects on each parameter were not significant anymore (reward sensitivity, $t(26) = -1.7$, $P_{\text{boot}} = 0.06$; punishment sensitivity, $t(26) = 1.7$, $P_{\text{boot}} = 0.07$).

Correlation analyses showed that higher insulin activity at follow-up 1 was significantly associated with fold change in liver fat, the change in reward learning and the food diary reported fold change in fat and saturated fatty acid intake, especially in the pons/midbrain (Fig. 2d) ($P < 0.05$; Extended Data Table 5). Lower insulin responsiveness in the fusiform gyrus 1 week after resuming a regular diet significantly correlated with the food diary reported fold change in carbohydrate intake and the hippocampal change in responsiveness to insulin correlated with the fold change in fat intake and saturated fatty acid intake ($P < 0.05$; Extended Data Table 5). Fractional anisotropy (FA) and mean diffusivity (MD) are summary measures of white matter diffusivity. The HCD group had significantly lower FA values mainly located on the inferior fronto-occipital fasciculus, genu of the corpus callosum and anterior corona radiata (Extended Data Fig. 3; $P < 0.05$; threshold-free cluster enhancement (TFCE)-corrected) as well as higher MD values in the superior corona radiata at follow-up 2 compared with baseline. No significant differences were observed at follow-up 1 compared with baseline. No group differences were observed at baseline for global FA values. However, significant group differences were observed for global MD values at baseline ($P < 0.05$). The control group showed higher MD values.

The current study demonstrates that brain insulin responsiveness adapts to short-term dietary changes after overconsumption of broadly available sweet and fatty ultra-processed snacks in addition to their regular diet, in healthy weight men, in the absence of changes in body weight, peripheral insulin sensitivity and food craving. Liver fat

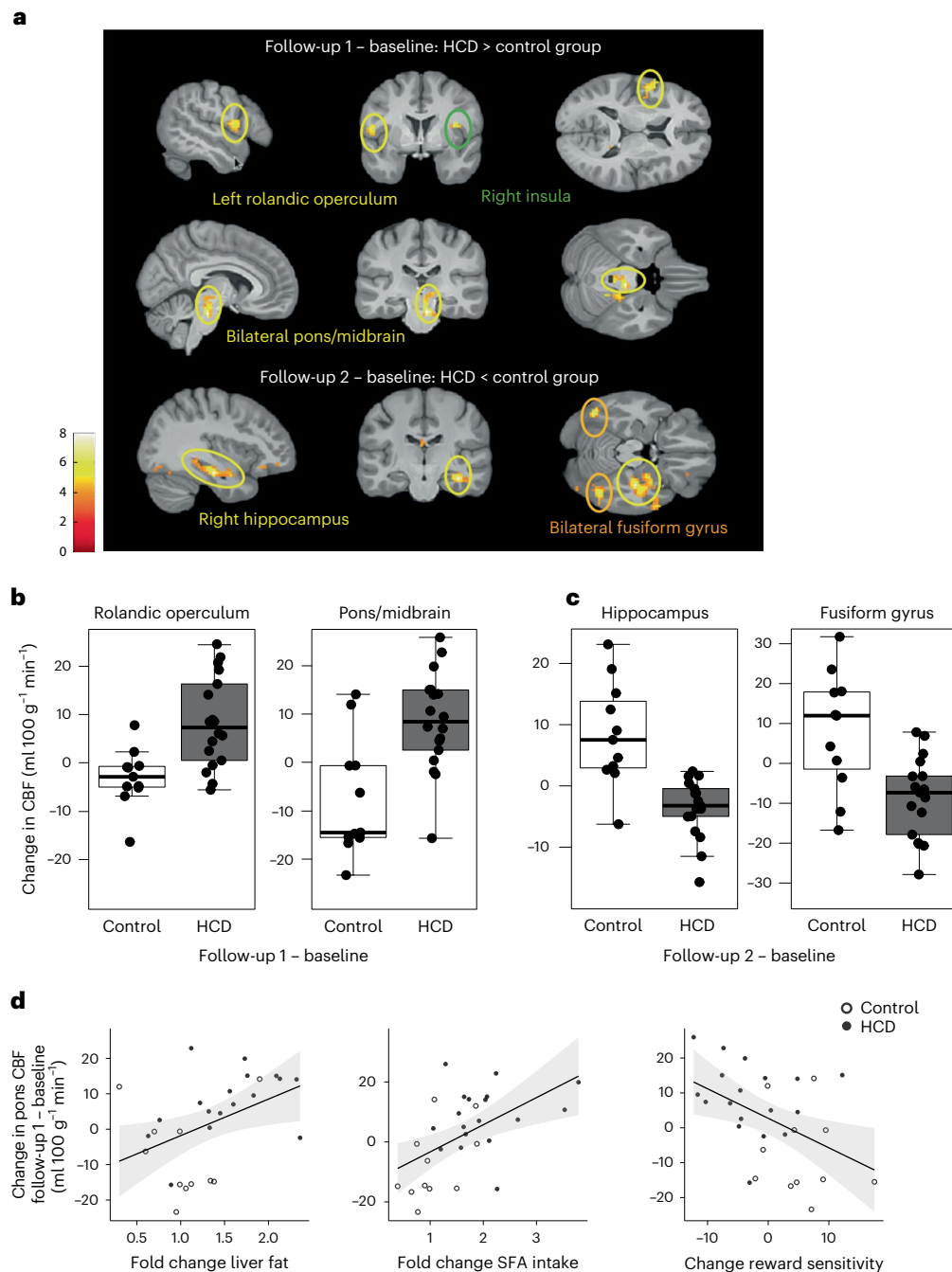


Fig. 2 | Disrupted brain insulin action after short-term overeating with calorie-rich snacks. a, Changes in brain insulin activity at follow-up 1 (directly after the 5-day HCD or regular diet) and follow-up 2 (1 week after resuming the regular diet) in HCD compared with the control group. Regions with significant changes in CBF after INI application in the HCD group compared with the control group and adjusted for the baseline measurement day are shown. Colour maps correspond to t -values ($P < 0.001$, uncorrected for display). **b**, Areas in the brain showing significantly higher insulin activity at follow-up 1 in the HCD compared with the control group adjusted for baseline measurement ($P_{\text{FWE}} < 0.05$, whole-brain cluster level corrected). $n = 29$ at baseline and follow-up 1. **c**, Areas in the brain showing significantly lower insulin activity at follow-up 2 in the HCD

compared with the control group adjusted for baseline measurement day ($P_{\text{FWE}} < 0.05$, whole-brain cluster level corrected). $n = 29$ at baseline, $n = 28$ at follow-up 2. Box plots show at the centre the median values indicated by thick horizontal lines; upper and lower hinges correspond to first and third quartiles (25th and 75th percentiles). The whiskers extend from the hinges to the minimum and maximum value, which is $1.5 \times$ interquartile range of the hinge. **d**, Higher brain insulin responsiveness at follow-up 1 (adjusted for the baseline visit) significantly correlated with the fold change in liver fat ($n = 28$; $r = 0.434$, $P = 0.02$), the food diary reported fold change in saturated fatty acid (SFA) intake ($n = 29$; $r = 0.531$, $P = 0.003$) and the change in reward sensitivity ($n = 29$) ($r = -0.460$, $P = 0.01$) at follow-up 1 adjusted for baseline.

content, however, substantially increased after this HCD, which was directly related to the initially augmented response to brain insulin of food reward pathways. Moreover, reward learning was also disrupted as indicated by a decreased sensitivity for rewards and increased sensitivity for punishments. These initial alterations normalized 1 week after

participants returned to their regular diet. Notably, insulin sensitivity of cognitive-related brain regions and markers of brain integrity were lower in the HCD compared with the control group after the HCD group resumed their regular diet. These data suggest that a short-term HCD, rich in sugar and saturated fat, has prolonged effects on the brain that

outlast the time-frame of its consumption. Habitual daily intake of sweet and fatty snacks for 8 weeks has been shown to increase neural responses to food, while decreasing the preference for low-fat food independent of changes in body weight and metabolism¹¹. In persons with obesity-associated insulin resistance, higher responsiveness to insulin has been observed in the insular cortex¹² and midbrain¹³, similar to the increased response that we observed after HCD. Moreover, studies in people with obesity found poorer performance in dopamine-dependent reward-learning paradigms^{14,15}. We could identify a similar alteration in the present study in healthy weight men after overconsumption of high-caloric food, providing evidence that altered reward learning and increased activity of the reward associated brain regions to insulin may be present before weight gain. After resuming a normal diet, we found a diminished response to brain insulin in the hippocampus and fusiform gyrus in the HCD group. Insulin activity in these regions plays an important role in attenuating the neural response to visual food cues¹⁶ and memory processes³. Under healthy conditions, INI improves performance on learning and memory tasks³ and increases hippocampal blood flow¹⁷ and hippocampal functional connectivity^{18,19}. Of note, the diminished response to insulin in the hippocampus and fusiform gyrus outlasted the consumption of the HCD. Notably, hippocampal insulin resistance can develop independent of peripheral insulin sensitivity²⁰, as identified in rodent models²⁰ and in postmortem brain tissue of patients with Alzheimer's disease²¹. Likewise, in the current study, diminished brain insulin responsiveness in the hippocampus was present without notable perturbations in peripheral metabolism, suggesting that diet-induced changes in brain insulin responsiveness precede peripheral insulin resistance. Together, these findings add a novel facet to our understanding of the possible development of brain insulin resistance and suggest that the detrimental effects of a HCD persists even after cessation of the unhealthy nutritional stimulus. Initial evidence indicates that, particularly in women, hippocampal insulin sensitivity decreases with age¹⁷. Whether our findings can be extended to women needs to be investigated in future studies. Besides insulin resistance, there are a multitude of factors that substantially contribute to the pathophysiology of obesity. Particularly, abdominal obesity is a source of inflammation²² and dietary excess can trigger inflammation in the brain in the preclinical model, involving non-neural populations such as astrocytes, microglia and tanocytes in the hypothalamus^{23,24} as well as the orbitofrontal cortex²⁵. While less is known about inflammation in the brain in humans, initial imaging studies point to structures of the hypothalamus and reward pathways being vulnerable to obesity-associated inflammation^{26,27}. Likewise, in the current study, we found reductions in white matter integrity between reward and cognitive regions after participants resumed their regular diet, similar to changes in individuals with obesity²⁸. Based on the nature of the MRI signal, these alterations in white matter integrity are based on changes in brain water content, which is known to be mediated by obesity-associated inflammation²⁶. Whether systemic inflammation contributed to these changes cannot be answered in the current study. However, no changes in cytokines were observed immediately after the HCD. Clearly, further studies are needed to disentangle the role of brain insulin responsiveness and inflammation in the development of obesity and associated diseases, as subclinical low-grade inflammation is well known to affect metabolic regulation.

In conclusion, we show that short-term overeating with commonly used ultra-processed high-caloric snacks can trigger liver fat accumulation and short-term disrupted brain insulin action that outlast the time-frame of the HCD in men. We postulate that the brain response to insulin adapts to short-term changes in diet before weight gain and may facilitate the development of obesity and associated diseases.

The small sample size of our study limits the generatability of our results and may be the reason why we did not identify impairments in peripheral insulin sensitivity after the 5-day HCD. Furthermore, we did not investigate whole-body insulin sensitivity based on the gold

standard (hyperinsulinaemic euglycaemic clamp). Knudsen et al.²⁹ were able to observe changes in whole-body insulin sensitivity after just 3 days of overeating and physical inactivity, before changes in body weight²⁹. This could indicate that inactivity facilitates a more rapid decrease in peripheral insulin sensitivity than the HCD alone. Furthermore, with the current study design, we cannot disentangle the effect of excessive calories on the brain versus the influence of excessive calories of specific macronutrients. Whether excessive intake of healthy calories or physical inactivity impacts brain insulin activity is the subject of future studies. For follow-up 2, no liver fat measurement and no blood sampling during oGTT were available. Hence, we cannot conclude whether the liver fat accumulation, inflammation or free fatty acid species play an important role beyond the HCD. Also, the study duration was too short to evaluate long-term effects of the HCD. We investigated the effect of HCD exclusively in male participants. Sex-specific findings of insulin action on appetite, metabolism and memory have been reported³, which depend in part on the menstrual cycle¹⁰. It is likely that adaptations of brain insulin activity to diet additionally depend on hormonal fluctuations in women.

Methods

Participants

Twenty-nine male participants were aged 19–27 years, were healthy weight (BMI 19–25 kg m⁻²), nonsmokers, of stable weight for at least 3 months before the study visits, nondieters, not vegan or vegetarian dieters, without food allergies, exercising less than 2 h a week, not working at night, not taking medication, and with no history of diabetes, eating disorders, illicit drug use or other medical diagnoses. Gender was determined based on self-report and supported by testosterone measurements. In a nonrandomized controlled design, 18 participants were enrolled to participate in a 5-day HCD (snacks in addition to their regular diet) and 11 participants were enrolled as the control group (to maintain their regular diet with no additional calories). Data collection and analysis were not performed blind to the conditions of the experiments. Participants provided written informed consent in compliance with the University of Tübingen ethical committee. The study (813/2017BO2) received approval by the local ethics committee in January 2018 (Ethics Committee of the Medical Faculty of the Eberhard Karls University and the University Hospital Tübingen) and was conducted according to the relevant guidelines and regulations. The study is a basic experimental study involving humans and was registered at ClinicalTrials.gov (NCT03590561). A compensation of €600 was provided after completion of the study (total of 23 h over six visits).

A previous study investigating brain insulin action⁶, showed a large effect size of Cohen's $d > 1$ could be achieved with 18 participants per group to detect obesity-associated insulin resistance (healthy weight versus obese). Assuming a two-sided t -test of $\alpha = 0.05$ and 80% power, a sample size of at least 25 people was calculated for the total sample size.

Study overview

Brain insulin action was assessed by fMRI combined with intranasal administration of insulin to the brain before, directly after the HCD or regular diet, and 1 week afterwards. The timing of the follow-up visits was adapted to the first day of the consumption of the HCD. Food intake and physical activity were recorded during the course of the study. Moreover, participants underwent two five-point 75 g oGTTs according to the methods of Matsuda and DeFronzo³⁰ to assess peripheral insulin sensitivity, whole-body MRI for body fat distribution/intrahepatic fat content, and performed a reward-learning task (see Fig. 1 for study overview). For each study visit, participants arrived at the study centre at -08:00 after an overnight fast of 12 h. Blood samples were taken during the oGTT and once before each fMRI measurement. Participants were instructed by a nutritionist to record their food intake into a diary and provide pictures of all their meals and instructed to walk fewer than 4,000 steps a day, monitored using a Fitbit watch (Fitbit Inspire or Fitbit

Inspire HR; Fitbit LLC, USA). High-caloric snacks were provided to the participants based on palatability ratings obtained before the baseline visit. Only participants who habitually consumed high-caloric snacks (at least four times a week) were included.

High-caloric diet

Based on the participant specific palatability ratings, a nutritionist prepared packages for 5 days containing 1,500 kcal each with different snacks (including for example, Snickers, brownies and chips, with a nutritional composition equivalence of 47–50% fat and 40–45% carbohydrates; see Supplementary Table 1).

Food diaries

Participants in the HCD group completed food diaries on three consecutive days before the intervention, five consecutive days during the intervention, and again three consecutive days at the end of the assessment period before follow-up 2. The control group completed food diaries for three consecutive days at two time points corresponding to the time between the baseline/follow-up 1 and follow-up 2 visits. Diet composition was estimated with a validated software (DGE-PC 3.0; German Nutrition Society). In addition, all consumed food was photographed by the participants to validate the information provided in the diary.

Whole-body MRI for quantification of adipose tissue compartments

T1-weighted fast spin-echo images with a 1-cm slice thickness and an interslice gap of 1 cm were acquired from the entire body on a 3T whole-body scanner (Magnetom Vida; Siemens Healthineers) in the early morning after overnight fasting³¹. After MRI, single-voxel MR spectroscopy was performed in the posterior part of segment 7 of the liver for quantification of IHL, which was calculated by the ratio of lipid signal and water plus lipid signal³².

Whole-brain MRI measurement and preprocessing

Scanning was conducted at a 3T whole-body Siemens scanner (Magnetom Prisma) with a 20-channel head/neck coil. Brain insulin responsiveness was quantified by application of INI in combination with fMRI recordings. Measurements were performed under fasting conditions. After the basal measurement, 160 U insulin spray was administered intranasally (Insulin Actrapid; Novo Nordisk). After 30 min, a second fMRI measurement was performed. To acquire CBF maps, pulsed arterial spin labelling images with a PICORE-Q2TIPS sequence (proximal inversion with control for off-resonance effects—quantitative imaging of perfusion by using a single subtraction) using a frequency offset corrected inversion pulse and echo planar imaging readout for acquisition^{6,33}. In addition, high-resolution T1-weighted anatomical images were obtained. Image preprocessing was performed using the ASLtbx with SPM12 (Wellcome Trust Centre for Neuroimaging). Functional images were motion corrected, co-registered to the individual anatomical image and smoothed (full width half maximum 6 mm). Perfusion images were generated by calculating the control-tag differences by using surround subtraction. For accurate CBF quantification ($\text{ml } 100 \text{ g}^{-1} \text{ min}^{-1}$), we used unique M0 values extracted from a region of interest in the cerebrospinal fluid³⁴. We used the general kinetic model for absolute perfusion quantification. Recent reliability studies and our measurements show high reproducibility and reliability for CBF maps^{34,35}.

Diffusion-weighted images were acquired at each visit before INI administration, to investigate white matter integrity. An echo planar imaging sequence (70 axial slices, field of view of 220 mm², slice thickness of 2 mm, TE = 54 ms and TR = 6,500 ms) with 35 directions ($b = 1,000 \text{ s mm}^{-2}$) and GRAPPA acceleration factor 2 was acquired. Moreover, 11 interspersed nondiffusion weighted volumes (b0) were recorded. To improve signal-to-noise ratio two averages were performed. The measurement lasted a total of 8 min 3 s. Standard

preprocessing and statistical analyses were performed using FMRIB (Functional Magnetic Resonance Imaging of the Brains, Oxford University) Software Library (FSL v.6.0). For all FA images, a nonlinear registration in MNI152 space was conducted using the FMRIB58_FA template as target image. The mean FA image pooled over all participants and sessions was computed and the skeleton representing the main white matter tracts was created. Thereafter, the aligned four-dimensional skeletonized FA images were thresholded ($\text{FA} \geq 0.2$) to reduce partial volume effects. For the nonlinear registration of the MD images into MNI space, the transformation parameters of the FA images were applied and skeletonized. One participant was excluded from the analyses because of imperfect slice positioning cutting parts of the white matter tracts.

Statistics

Unless otherwise stated, data are presented as mean \pm s.d. The primary analysis was to assess insulin-induced changes in brain activity before (baseline) and twice after the intervention (follow-up 1 and follow-up 2). To this end, the absolute change of CBF of each participant before and after INI spray application was used for further statistics (ΔCBF , CBF 30 min after nasal spray – CBF before nasal spray). Whole-brain analyses were performed using a voxel-wise approach in SPM12. ΔCBF of the baseline measurement day was subtracted from the follow-up visits ($\Delta\text{CBF}_{\text{follow-up } 1/2} - \Delta\text{CBF}_{\text{baseline}}$) and entered into a flexible factorial design to investigate the difference in brain insulin responsiveness between the HCD and control groups at follow-up 1 and follow-up 2, while taking into account within-subject variability (within-subject factors, subject ID and visit (follow-up 2 and follow-up 1); between-subject factor, group (HCD and control)). A statistical threshold of $P < 0.001$ uncorrected and $P_{\text{FWE}} < 0.05$ cluster level corrected for multiple comparisons was applied on a whole-brain level.

To investigate differences in white matter integrity between the HCD and control group, FA and MD values from the baseline to follow-up 1 and follow-up 2 (follow-up 1/2 – baseline) were calculated for each participant on the skeletonized data using fslmaths. A two-sample unpaired *t*-test was performed between the HCD and the control group for FA and MD values, respectively. We included the global FA/MD values as a covariate of no interest. For tract-based spatial statistics, we used the module randomize in FSL, which is a nonparametric permutation test for inference on statistical maps³⁶. For detecting significant clusters corrected for multiple comparisons, we selected the TFCE method optimized for TBSS analyses³⁷. Statistical maps were thresholded at $P < 0.05$ (TFCE corrected). The number of permutations was set to 5,000. Tract labels were assigned using JHU ICBM-DTI-81 white matter labels or the HCP white matter probability tracts.

Secondary analyses were conducted using R (v.4.3.3.). Groups, visits as well as group-by-visit interactions were tested by linear mixed-effects models employing the lmer function of the lme4 package in R. Participants were included as random factors to account for within-subject correlations. Groups and visits were considered as fixed effects. Normal distribution was investigated by visual inspection and QQ plots. In exploratory analyses, correlations were used to associate metabolic and behavioural changes with changes in brain insulin action ($P < 0.05$ uncorrected for multiple comparisons).

Questionnaires

Participants reported impulsivity (Barratt impulsiveness scale³⁸), eating behaviour (food craving questionnaire – trait)³⁹ and the three-factor eating questionnaire⁴⁰; German version, fragebogen zum essverhalten⁴¹). Furthermore, eating disorders (eating disorder examination⁴²), depression (Becks-depressions-inventar⁴³) and psychiatric disease (patient health questionnaire⁴⁴) were ruled out. Before and after the INI, participants rated their mood (positive and negative affect schedule questionnaire⁴⁵) and their subjective feeling of hunger on a visual analogue scale (0, not hungry at all to 10, very hungry).

Go/no-go learning task

We investigated reward learning with an established valence-dependent go/no-go learning paradigm⁴⁶. Participants were asked to learn correct approach (go) or inhibitory (no-go) responses to cues that predicted reward or punishment. With this task, participants learned state-action contingencies and received rewards or punishments. Each trial consisted of three stages; 240 trials in total, consisting of 120 go trials and 120 no-go trials, each with 60 trials for each condition (for example, win or avoid loss); the task duration was 15 min. Using a laptop computer, fractal cues (state) were presented out of a set of four different fractals per session. Fractals were randomized to one of the four possible combinations of the go × win two-factorial design of the task. Participants completed a target detection task and either respond by pressing a key (go) or withhold their response (no-go). The outcome of the state-action combination is visualized on the screen, which was either a win (5 cents), punishment (−5 cents) or an omission (no win/punishment, 0 cents). Using trial and error, participants learned which action following each fractal was best in terms of maximizing wins or minimizing losses. Outcomes were presented probabilistically, as follows: 80% chance to win after correct state-action sequences; 20% chance to win after incorrect sequences for rewarded trials; 80% chance to avoid losses after correct; and 20% chance to avoid losses after incorrect sequences for punished trials. Participants were told about the probabilistic nature of the task and that either go or no-go responses could be correct for a given fractal. There was no change in the contingencies over time. To ensure that participants understood the task, they performed a practice run at the beginning.

Reinforcement learning model

We used computational modelling to test the effects of the HCD on specific processes of value-based decision-making. To this end, we fit previously reported reinforcement learning models that are extensions of standard Q-learning models⁴⁶. In brief, specific action (a) values (Q) are updated for the shown stimulus (s) at each trial t with the Rescorla-Wagner rule:

$$Q_t(s_t, a_t) = Q_{t-1}(s_t, a_t) + \alpha(\rho r_t - Q_{t-1}(s_t, a_t)).$$

The speed of learning is modified by the learning rate α ($\alpha \in [0,1]$) and individual reward sensitivity is scaled by ρ , a free, positive parameter. Obtained rewards r_t are coded as −1, 1 or 0 if participants received a punishment, reward or neither, respectively. To account for Pavlovian effects on learning, action-independent values (V) for each stimulus are learned with the same Rescorla-Wagner rule to indicate whether a stimulus leads to punishment or reward:

$$V(s_t) = V_{t-1}(s_t) + \alpha(\rho r_t - V_{t-1}(s_t))$$

Both action values (Q) and stimulus values (V) are then combined to action weights (W) at each trial:

$$W_t(a, s) = \begin{cases} Q_t(a, s) + b + \pi V_t(s), & a = \text{go} \\ Q_t(a, s), & \text{else} \end{cases}$$

Here, b (>0) reflects the constant tendency to choose the go option and Pavlovian tendencies are parameterized by π , a positive free parameter that captures impaired learning in trials with incongruent Pavlovian and instrumental behaviour (for example, go-to-avoid punishment). Last, the action probability (p) at each trial is determined using a softmax function where a noise parameter ($\xi \in [0, 1]$) scales how much influence learned values have on decisions:

$$p(a_t|s_t) = \left[\frac{\exp(W(a_t|s_t))}{\sum_a \exp(W(a|s_t))} \right] \times \xi + \left(\frac{1-\xi}{2} \right)$$

In addition, we fit two further models disentangling valence specific effects by estimating either reward sensitivity, or reward sensitivity and learning rate separately for reward and punishment. To test whether valence effects were specific for reward sensitivity versus learning rates⁴⁷, we also explored a model that separated learning rates, but not reward sensitivity based on outcome valence. As the model that included a valenced learning rate did not converge, it precluded further analyses. As previously described, we used hierarchical expectation maximization to fit the models⁴⁸. Using this method, individual parameters and the group distributions of the parameters are estimated iteratively, so that at each iteration, the current group-level distributions are used as priors for individual parameter estimation (Laplace approximation). Consequently, group-level distributions are updated integrating the new individual estimates and their uncertainty. To avoid systematic bias, we treated each repeated sessions (baseline, follow-up 1 and follow-up 2) as an independent measurement. To prevent exaggerating differences between both groups, we fit one underlying distribution over all participants and repeated measurements. We compared models using group-level integrated BIC (iBIC⁴⁸), which combines model fit and model complexity across all measurements. To constrain parameters to their theoretical range, we log-transformed reward sensitivity and Pavlovian bias and used an inverse sigmoid transformation for the learning rate and irreducible noise.

We evaluated intervention effects by comparing changes in parameter estimates between the HCD and the control group using independent-sample t -tests with a significance threshold of $P < 0.05$ (two-tailed). As model parameters might not be normally distributed, we used bootstrapping with 1,000 samples to compare changes in parameter estimates at follow-up 1 and follow-up 2 between groups. Moreover, we corrected for multiple comparisons across the six parameters in the winning computational model analysis using Bonferroni correction. We performed data analyses using MATLAB v.2016a (computational model).

To evaluate whether HCD alters reward and punishment sensitivity, we fitted computational reward-learning models⁴⁶ that dissociate sensitivity in response to wins or losses as outcomes. In line with Guitart-Masip et al.⁴⁹, a model including six parameters with valenced (reward/punishment) reward sensitivities provided a better model fit compared with the standard five-parameter model ($\Delta\text{iBIC} = -184$). In this model, HCD had opposing effects on reward and punishment sensitivity at both post intervention time points (Extended Data Fig. 2). We also explored a model only including a valenced learning rate but not a valenced reward sensitivity as previously described⁴⁷. However, while this model provided a slightly better model fit compared with the winning model ($\Delta\text{iBIC} = -74$) at the group level, it only provided a more parsimonious account at the individual (iBIC) level for 23 out of 86 runs. Nonetheless, there were no significant differences between groups at both times, neither for the single reward sensitivity nor the valenced learning rates, indicating that effects were specific for reward sensitivity.

Detection of cytokines

Cytokines were quantified using a combination of Bio-Plex Pro Human Cytokine Plex Panels (Luminex; Bio-Rad Laboratories). Multiplex assay was performed on a Luminex 200 system in accordance with the manufacturer's instructions. Samples were measured at two different time points on different plates. Hence, values were time-point-normalized for statistical analyses.

Reporting summary

Further information on research design is available in the Nature Portfolio Reporting Summary linked to this article.

Data availability

Statistical maps of the brain effects are uploaded to Neurovault (<https://neurovault.org/collections/MYQHVMQE/>). Source data are provided with this paper.

Code availability

No custom code was used.

References

- DeFronzo, R. A. et al. Type 2 diabetes mellitus. *Nat. Rev. Dis. Primers* **1**, 15019 (2015).
- Kullmann, S. et al. Central nervous pathways of insulin action in the control of metabolism and food intake. *Lancet Diabetes Endocrinol.* **8**, 524–534 (2020).
- Hallschmid, M. Intranasal insulin. *J. Neuroendocrinol.* **33**, e12934 (2021).
- Kellar, D. & Craft, S. Brain insulin resistance in Alzheimer's disease and related disorders: mechanisms and therapeutic approaches. *Lancet Neurol.* **19**, 758–766 (2020).
- Scherer, T., Sakamoto, K. & Buettner, C. Brain insulin signalling in metabolic homeostasis and disease. *Nat. Rev. Endocrinol.* **17**, 468–483 (2021).
- Kullmann, S. et al. Selective insulin resistance in homeostatic and cognitive control brain areas in overweight and obese adults. *Diabetes Care* **38**, 1044–1050 (2015).
- Kullmann, S. et al. Brain insulin sensitivity is linked to adiposity and body fat distribution. *Nat. Commun.* **11**, 1841 (2020).
- Rebelos, E., Nummenmaa, L., Dadson, P., Latva-Rasku, A. & Nuutila, P. Brain insulin sensitivity is linked to body fat distribution: the positron emission tomography perspective. *Eur. J. Nucl. Med. Mol. Imaging* **48**, 966–968 (2021).
- Gruber, J. et al. Impact of insulin and insulin resistance on brain dopamine signalling and reward processing - An underexplored mechanism in the pathophysiology of depression? *Neurosci. Biobehav. Rev.* **149**, 105179 (2023).
- Hummel, J. et al. Brain insulin action on peripheral insulin sensitivity in women depends on menstrual cycle phase. *Nat. Metab.* **5**, 1475–1482 (2023).
- Edwin Thanarajah, S. et al. Habitual daily intake of a sweet and fatty snack modulates reward processing in humans. *Cell. Metab.* **35**, 571–584 e576 (2023).
- Wingrove, J. O. et al. Intranasal insulin administration decreases cerebral blood flow in cortico-limbic regions: a neuropharmacological imaging study in normal and overweight males. *Diabetes Obes. Metab.* **23**, 175–185 (2021).
- Tiedemann, L. J. et al. Central insulin modulates food valuation via mesolimbic pathways. *Nat. Commun.* **8**, 16052 (2017).
- Kroemer, N. B. & Small, D. M. Fuel not fun: reinterpreting attenuated brain responses to reward in obesity. *Physiol. Behav.* **162**, 37–45 (2016).
- Gill, H. et al. The impact of overweight/obesity on monetary reward processing: a systematic review. *J. Psychiatr. Res.* **137**, 456–464 (2021).
- Guthoff, M. et al. Insulin modulates food-related activity in the central nervous system. *J. Clin. Endocrinol. Metab.* **95**, 748–755 (2010).
- Wagner, L. et al. Brain insulin responsiveness is linked to age and peripheral insulin sensitivity. *Diabetes Obes. Metab.* **25**, 2171–2180 (2023).
- Kullmann, S. et al. Intranasal insulin enhances brain functional connectivity mediating the relationship between adiposity and subjective feeling of hunger. *Sci. Rep.* **7**, 1627 (2017).
- Zhang, H. et al. Intranasal insulin enhanced resting-state functional connectivity of hippocampal regions in type 2 diabetes. *Diabetes* **64**, 1025–1034 (2015).
- Grillo, C. A., Woodruff, J. L., Macht, V. A. & Reagan, L. P. Insulin resistance and hippocampal dysfunction: disentangling peripheral and brain causes from consequences. *Exp. Neurol.* **318**, 71–77 (2019).
- Talbot, K. et al. Demonstrated brain insulin resistance in Alzheimer's disease patients is associated with IGF-1 resistance, IRS-1 dysregulation, and cognitive decline. *J. Clin. Invest.* **122**, 1316–1338 (2012).
- Alexopoulos, N., Katritsis, D. & Raggi, P. Visceral adipose tissue as a source of inflammation and promoter of atherosclerosis. *Atherosclerosis* **233**, 104–112 (2014).
- Garcia-Caceres, C. et al. Role of astrocytes, microglia, and tanycytes in brain control of systemic metabolism. *Nat. Neurosci.* **22**, 7–14 (2019).
- Porniece Kumar, M. et al. Insulin signalling in tanycytes gates hypothalamic insulin uptake and regulation of AgRP neuron activity. *Nat. Metab.* **3**, 1662–1679 (2021).
- Lau, B. K. et al. Obesity-induced astrocyte dysfunction impairs heterosynaptic plasticity in the orbitofrontal cortex. *Cell Rep.* **36**, 109563 (2021).
- Kullmann, S. et al. Investigating obesity-associated brain inflammation using quantitative water content mapping. *J. Neuroendocrinol.* **32**, e12907 (2020).
- Dorfman, M. D. & Thaler, J. P. Hypothalamic inflammation and gliosis in obesity. *Curr. Opin. Endocrinol. Diabetes Obes.* **22**, 325–330 (2015).
- Daoust, J. et al. White matter integrity differences in obesity: a meta-analysis of diffusion tensor imaging studies. *Neurosci. Biobehav. Rev.* **129**, 133–141 (2021).
- Knudsen, S. H. et al. Changes in insulin sensitivity precede changes in body composition during 14 days of step reduction combined with overfeeding in healthy young men. *J. Appl. Physiol.* **113**, 7–15 (2012).
- Matsuda, M. & DeFronzo, R. A. Insulin sensitivity indices obtained from oral glucose tolerance testing: comparison with the euglycemic insulin clamp. *Diabetes Care* **22**, 1462–1470 (1999).
- Wurslin, C. et al. Topography mapping of whole body adipose tissue using a fully automated and standardized procedure. *J. Magn. Reson. Imaging* **31**, 430–439 (2010).
- Machann, J. et al. Hepatic lipid accumulation in healthy subjects: a comparative study using spectral fat-selective MRI and volume-localized 1H-MR spectroscopy. *Magn. Reson. Med.* **55**, 913–917 (2006).
- Kullmann, S. et al. Empagliflozin improves insulin sensitivity of the hypothalamus in humans with prediabetes: a randomized, double-blind, placebo-controlled, phase 2 trial. *Diabetes Care* **45**, 398–406 (2022).
- Kullmann, S. et al. Exercise restores brain insulin sensitivity in sedentary adults who are overweight and obese. *JCI Insight* **7**, e161498 (2022).
- Ssali, T. et al. Mapping long-term functional changes in cerebral blood flow by arterial spin labeling. *PLoS ONE* **11**, e0164112 (2016).
- Winkler, A. M., Ridgway, G. R., Webster, M. A., Smith, S. M. & Nichols, T. E. Permutation inference for the general linear model. *Neuroimage* **92**, 381–397 (2014).
- Smith, S. M. & Nichols, T. E. Threshold-free cluster enhancement: addressing problems of smoothing, threshold dependence and localisation in cluster inference. *Neuroimage* **44**, 83–98 (2009).
- Meule, A., Vögele, C. & Kübler, A. Psychometrische evaluation der Deutschen Barratt Impulsivness Scale-Kurzversion (BIS-15). *Diagnostica* **57**, 126–133 (2011).
- Meule, A., Hermann, T. & Kübler, A. A short version of the Food Cravings Questionnaire-Trait: the FCQ-T-reduced. *Front. Psychol.* **5**, 190 (2014).
- Stunkard, A. J. & Messick, S. The three-factor eating questionnaire to measure dietary restraint, disinhibition and hunger. *J. Psychosom. Res.* **29**, 71–83 (1985).
- Pudel, V. & Westenhöfer, J. *Fragebogen zum Essverhalten (FEV): Handanweisung* (Verlag für Psychologie Hogrefe, 1989).

42. Hilbert, A. & Tuschen-Caffier, B. *Eating Disorder Examination: Deutschsprachige Übersetzung* (Verlag für Psychotherapie, 2006).
43. Hautzinger, M., Keller, F. & Kühner, C. *BDI-II. Beck Depression Inventar Revision-Manual* (Harcourt Test Services, 2006).
44. Löwe, B., Spitzer, R.L., Zipfel, S. & Herzog, W. *PHQ-D* (Gesundheitsfragebogen für Patienten, 2002).
45. Krohne, H. W., Egloff, B., Kohlmann, C.-W. & Tausch, A. Untersuchung der deutschen Form der Positiven und Negativen Affect Schedule (PANAS). *Diagnostica* **42**, 139–156 (1996).
46. Guitart-Masip, M. et al. Go and no-go learning in reward and punishment: interactions between affect and effect. *Neuroimage* **62**, 154–166 (2012).
47. Kühnel, A. et al. Stimulation of the vagus nerve reduces learning in a go/no-go reinforcement learning task. *Eur. Neuropsychopharmacol.* **35**, 17–29 (2020).
48. Huys, Q. J. et al. Disentangling the roles of approach, activation and valence in instrumental and pavlovian responding. *PLoS Comput. Biol.* **7**, e1002028 (2011).
49. Guitart-Masip, M. et al. Differential, but not opponent, effects of L-DOPA and citalopram on action learning with reward and punishment. *Psychopharmacology* **231**, 955–966 (2014).
50. Preissl, H. Figure 1. *BioRender* <https://BioRender.com/d74p651> (2025).

Acknowledgements

The studies were supported in part by a grant (01GI0925) from the Federal Ministry of Education and Research to the German Center for Diabetes Research and by a grant from the State of Brandenburg (grant 82DZD00302) to A. Kleinridders.

Author contributions

S.K. designed the trial, researched and analysed the data, supervised the project and drafted the paper. L.W., R.H., A. Kühnel, L.S., C.D. and J.M. researched the data. R.V. researched and analysed data. A.F. and N.S. contributed to discussions. H.P., N.B.K., M.H. and A. Kleinridders contributed to the design of the trial and discussed data. A.L.B. contributed to discussions and drafted the paper. All authors contributed to discussions and approved the final version of the paper.

Funding

Open access funding provided by Helmholtz Zentrum München - Deutsches Forschungszentrum für Gesundheit und Umwelt (GmbH).

Competing interests

M.H. reports research grants from Boehringer Ingelheim and Sanofi to the University Hospital of Tübingen; participation in advisory board for Boehringer Ingelheim, Sanofi and Amryt; and lecture fees from Amryt, Novartis, Sanofi, Eli Lilly, Novo Nordisk and Boehringer Ingelheim. The other authors declare no competing interests.

Additional information

Extended data is available for this paper at <https://doi.org/10.1038/s42255-025-01226-9>.

Supplementary information The online version contains supplementary material available at <https://doi.org/10.1038/s42255-025-01226-9>.

Correspondence and requests for materials should be addressed to Stephanie Kullmann.

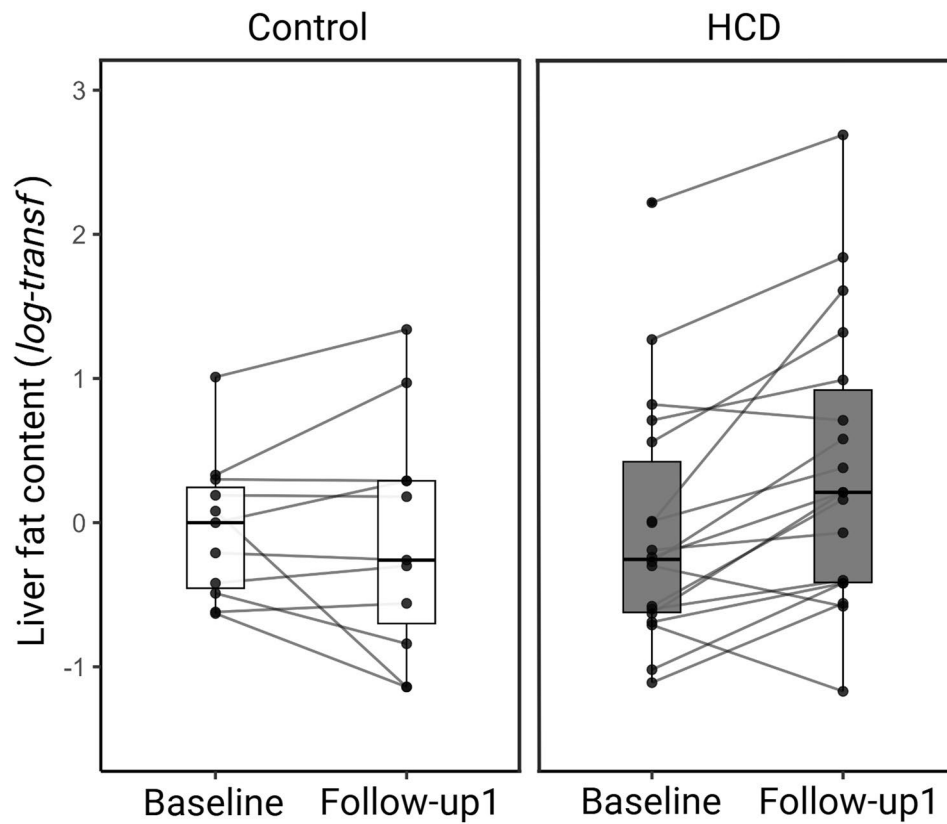
Peer review information *Nature Metabolism* thanks Alexandra Di Feliceantonio, Annette Horstmann and the other, anonymous, reviewer(s) for their contribution to the peer review of this work. Primary Handling Editor: Yanina-Yasmin Pesch, in collaboration with the *Nature Metabolism* team.

Reprints and permissions information is available at www.nature.com/reprints.

Publisher's note Springer Nature remains neutral with regard to jurisdictional claims in published maps and institutional affiliations.

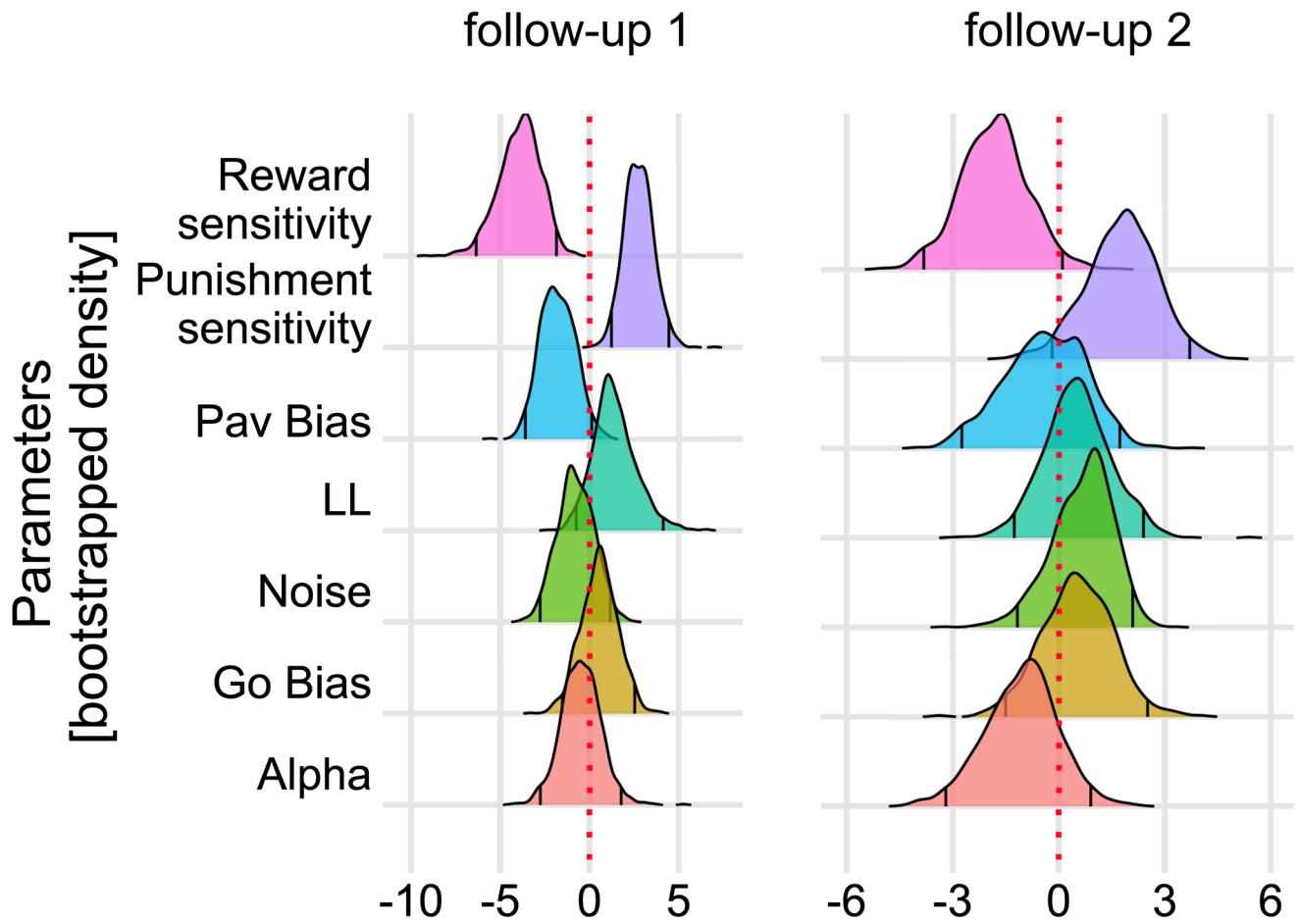
Open Access This article is licensed under a Creative Commons Attribution 4.0 International License, which permits use, sharing, adaptation, distribution and reproduction in any medium or format, as long as you give appropriate credit to the original author(s) and the source, provide a link to the Creative Commons licence, and indicate if changes were made. The images or other third party material in this article are included in the article's Creative Commons licence, unless indicated otherwise in a credit line to the material. If material is not included in the article's Creative Commons licence and your intended use is not permitted by statutory regulation or exceeds the permitted use, you will need to obtain permission directly from the copyright holder. To view a copy of this licence, visit <http://creativecommons.org/licenses/by/4.0/>.

© The Author(s) 2025



Extended Data Fig. 1 | Liver fat content in the control and high-caloric diet group (HCD) at baseline and 5-days after the high-caloric or regular diet intervention (follow-up 1). Liver fat content increased in the HCD group: baseline versus follow-up 1: $p = 0.005$, while it did not change in the control group

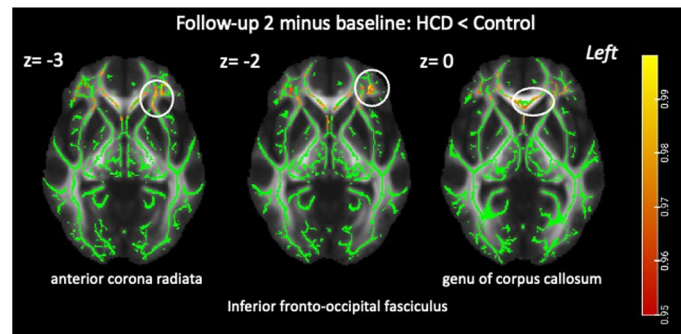
($p = 0.958$). Presented are box plots with whiskers indicating 1.5 interquartile range and line diagram; Control: $N = 11$ at baseline and follow-up 1; HCD: $N = 17$ at baseline and $N = 18$ follow-up 1. Abbreviations: HCD, high-caloric diet group.



HCD compared to control group

Extended Data Fig. 2 | HCD reduced reward sensitivity and increased punishment sensitivity. Bootstrapped density plots of the difference between groups in changes of parameter estimates at follow-up 1 and follow-up 2

compared to baseline (pre), respectively. Lines indicate 95% confidence intervals. HCD = high-caloric diet group; RewS = Reward Sensitivity, Pav = Pavlovian, LL = log-likelihood.



Extended Data Fig. 3 | Change in white matter organization at follow-up 2. Change in white matter organization at follow-up 2 in the high-caloric diet compared to the control group. The panel shows the fractional anisotropy skeleton (in green) representing the major white matter tracts of all participants overlaid on a MNI standard brain. White matter fibre tracts showing a significantly lower fractional anisotropy (FA) at follow-up 2 in the high-caloric

diet compared to the control group are shown in red, orange and yellow ($p\text{-corr} < 0.05$). Lower FA values are mainly located on inferior fronto-occipital fasciculus, genu of the corpus callosum and anterior corona radiata (white circles). Colorbar represents 1-p value (tfce-corrected). Tracts in yellow displayed smaller p value or more significant results. $N = 27$.

Extended Data Table 1 | Food Diary

		Baseline		Follow-up 1		Follow-up 2	
		mean	STD	mean	STD	mean	STD
Energy intake (kcal)	Control group	2557	621			2178	562
	HCD group	2617	735	3791*	589	2341	693
	HCD Baseline vs. Follow-up 1	Estimate = 1174.04, CI [945.72 1402.34], p < 0.001					
Fat [%]	Control group	37	4			39	9
	HCD group	38	7	44*	3	38	9
	HCD Baseline vs. Follow-up 1	Estimate = 6.12, CI [2.41 9.84], p = 0.002					
Fat [g]	Control group	107	28			98	36
	HCD group	112	43	185*	33	98	36
	HCD Baseline vs. Follow-up 1	Estimate = 72.86, CI [57.35 88.34], p < 0.001					
Carbohydrates [%]	Control group	45	4			44	7
	HCD group	44	9	44	4	45	10
Carbohydrates [g]	Control group	289	82			233	71
	HCD group	285	91	402*	69	258	97
	HCD Baseline vs. Follow-up 1	Estimate = 1117.39, CI [85.35 149.43], p < 0.001					
Proteins [%]	Control group	15	2			15	2
	HCD group	15	3	11*	1	16	4
	HCD Baseline vs. Follow-up 1	Estimate = -3.99, CI [-5.66 -2.32], p < 0.001					
Proteins [g]	Control group	93	20			80	25
	HCD group	97	33	113*	29	92	50
Saturated fatty acids [g]	Control group	31	12			33	13
	HCD group	41	17	76*	14	40	13
	HCD Baseline vs. Follow-up 1	Estimate = 34.59, CI [27.76 41.42], p < 0.001					
Monounsaturated fatty acids [g]	Control group	29	8			28	12
	HCD group	37	18	48*	18	33	20
	HCD Baseline vs. Follow-up 1	Estimate = 10.81, CI [2.87 18.75], p = 0.009					
Polyunsaturated fatty acids [g]	Control group	17	8			11	6
	HCD group	17	13	18	9	12	7
Fiber [g]	Control group	21	11			16	11
	HCD group	23	12	26*	12	18	7
	HCD Baseline vs. Follow-up 1	Estimate = 3.21, CI [0.52 5.90], p = 0.02					

*significant within group differences for HCD group from baseline to follow-up 1 visit, based on linear mixed effects models (LMER) employing the lmer function of the lme4 package in R. The control group showed no differences between visits (p>0.05). No group differences were found for baseline and follow-up 2 (p>0.05).

Extended Data Table 2 | State Questionnaires on Brain MRI day in the fasted state

		Baseline		Follow-up 1		Follow-up 2	
		mean	STD	mean	STD	mean	STD
Desire to eat (VAS)	Control group	4.35	2.58	3.79	2.42	4.32	2.92
	HCD group	5.50	2.15	4.45	2.92	4.78	2.79
FCQS total scale	Control group	32.54	9.02	29.00	7.22	31.45	11.48
	HCD group	36.61	9.64	37.44	10.11	36.70	9.77
PANAS positive affect	Control group	27.18	6.53	24.30	5.12	20.45	4.84
	HCD group	27.88	5.68	24.66	8.25	24.05	8.12
PANAS negative affect	Control group	13.27	3.13	11.90	2.66	11.27	1.95
	HCD group	11.29	1.26	11.38	1.41	10.68	0.94
Abbreviations: FCQS, food craving questionnaire state; PANAS, positive and negative affect schedule; VAS, visual analogue scale							

Extended Data Table 3 | Inflammatory markers

	Control (n=11)		HCD (n=18)	
	Baseline	Follow-up 1	Baseline	Follow-up 1
VCAM	1.020 ± 0.109	1.003 ± 0.162	0.987 ± 0.287	0.998 ± 0.430
ICAM	0.991 ± 0.202	0.984 ± 0.184	1.006 ± 0.308	1.010 ± 0.341
Osteopontin	1.014 ± 0.246	1.039 ± 0.454	0.991 ± 0.533	0.975 ± 0.466
sTNF-R1	0.979 ± 0.354	0.983 ± 0.338	1.013 ± 0.278	1.011 ± 0.220
sTNF-R2	1.037 ± 0.435	1.040 ± 0.532	0.976 ± 0.336	0.973 ± 0.241
Hu IP-10	1.123 ± 0.742	1.158 ± 1.545	0.925 ± 0.503	0.898 ± 0.613
Hu MCP-1	0.945 ± 0.435	0.999 ± 0.455	1.033 ± 0.362	1.001 ± 0.389
Hu MIP-1b	0.997 ± 0.530	1.010 ± 0.342	1.002 ± 0.175	0.994 ± 0.087
Hu RANTES	0.991 ± 0.098	1.003 ± 0.098	1.006 ± 0.137	0.998 ± 0.162
Hu IFN-g	0.993 ± 0.322	0.959 ± 0.399	1.004 ± 0.325	1.027 ± 0.477
Hu-TNF-a	0.889 ± 0.625	0.991 ± 0.800	1.068 ± 0.240	1.006 ± 0.374
Hu-IL-18	1.075 ± 0.637	1.099 ± 0.759	0.954 ± 0.281	0.936 ± 0.335
Hu MIG	1.014 ± 0.458	1.186 ± 1.949	0.992 ± 0.390	0.880 ± 1.015

Values are time-point normalized and presented in arbitrary units.

Extended Data Table 4 | Changes in brain insulin activity (CBF) from before to after the intervention

Brain region	Hemi	MNI Coordinates			Peak-t	Cluster size (k)	p _{FWE} peak/cluster
		x	y	z			
Follow-up 1 minus baseline							
HCD > Control							
Region in pons/midbrain	R	6	-25	-25	6.83	220	0.007/<0.001
Insula	R	36	5	17	6.80	19	0.007/0.357
Rolandic Operculum	L	-54	2	11	5.53	67	0.174/0.006
HCD < Control							
No differential activation	--	--	--	--	--		--
Follow-up 2 minus baseline							
HCD > Control							
No differential activation	--	--	--	--	--		--
HCD < Control							
Hippocampus	R	36	-19	-19	7.94	270	<0.001/<0.001
Fusiform gyrus	R	45	-58	-22	6.74	83	0.009/0.002
Fusiform gyrus	L	-45	64	-19	6.68	28	0.154/0.012

CBF, cerebral blood flow; Hemi = Hemisphere, R = right; p value FWE corrected using whole-brain peak/ cluster correction

Extended Data Table 5 | Correlation between change in brain insulin responsiveness and metabolic and behavioural changes

Changes in	Follow-up 1 minus baseline			Follow-up 2 minus baseline	
	Insula	Rolandic Operculum	Pons/ Midbrain	Fusiform gyrus	Hippocampus
Liver fat (Follow-up1/baseline)	r=0.425, p=0.02	r=0.434, p=0.02	r=0.434, p=0.02	ns	ns
Reward sensitivity (Follow-up1 minus baseline)	ns	ns	r=-0.460, p=0.01	ns	ns
Punishment sensitivity (Follow-up1 minus baseline)	ns	ns	r=0.381, p=0.04	ns	ns
Fat intake (Baseline or Follow-up1 for HCD/ Follow-up2)	r=0.385, p=0.04	ns	r=0.400, p=0.03	ns	r= -0.417, p=0.02
Saturated fatty acid intake (Baseline or Follow-up1 for HCD/ Follow-up2)	r=0.359, p=0.05	ns	r=0.531, p=0.003	ns	ns
Carbohydrate intake (Baseline or Follow-up1 for HCD/ Follow-up2)	ns	ns	ns	r= -0.400, p=0.03	

Pearson correlations were used to associate metabolic changes and behavioral changes with changes in brain insulin responsiveness at follow-up adjusted for baseline ($p < 0.05$ uncorrected for multiple comparisons); ns= not significant.

Reporting Summary

Nature Portfolio wishes to improve the reproducibility of the work that we publish. This form provides structure for consistency and transparency in reporting. For further information on Nature Portfolio policies, see our [Editorial Policies](#) and the [Editorial Policy Checklist](#).

Statistics

For all statistical analyses, confirm that the following items are present in the figure legend, table legend, main text, or Methods section.

n/a | Confirmed

- The exact sample size (n) for each experimental group/condition, given as a discrete number and unit of measurement
- A statement on whether measurements were taken from distinct samples or whether the same sample was measured repeatedly
- The statistical test(s) used AND whether they are one- or two-sided
Only common tests should be described solely by name; describe more complex techniques in the Methods section.
- A description of all covariates tested
- A description of any assumptions or corrections, such as tests of normality and adjustment for multiple comparisons
- A full description of the statistical parameters including central tendency (e.g. means) or other basic estimates (e.g. regression coefficient) AND variation (e.g. standard deviation) or associated estimates of uncertainty (e.g. confidence intervals)
- For null hypothesis testing, the test statistic (e.g. F , t , r) with confidence intervals, effect sizes, degrees of freedom and P value noted
Give P values as exact values whenever suitable.
- For Bayesian analysis, information on the choice of priors and Markov chain Monte Carlo settings
- For hierarchical and complex designs, identification of the appropriate level for tests and full reporting of outcomes
- Estimates of effect sizes (e.g. Cohen's d , Pearson's r), indicating how they were calculated

Our web collection on [statistics for biologists](#) contains articles on many of the points above.

Software and code

Policy information about [availability of computer code](#)

Data collection

Data analysis

For manuscripts utilizing custom algorithms or software that are central to the research but not yet described in published literature, software must be made available to editors and reviewers. We strongly encourage code deposition in a community repository (e.g. GitHub). See the Nature Portfolio [guidelines for submitting code & software](#) for further information.

Data

Policy information about [availability of data](#)

All manuscripts must include a [data availability statement](#). This statement should provide the following information, where applicable:

- Accession codes, unique identifiers, or web links for publicly available datasets
- A description of any restrictions on data availability
- For clinical datasets or third party data, please ensure that the statement adheres to our [policy](#)

Source data related to the tables, figures and extended data figures and tables are provided in this paper. Statistical maps of the brain effects are uploaded to neurovault (<https://neurovault.org/collections/MYQHVMQE/>).

Research involving human participants, their data, or biological material

Policy information about studies with [human participants or human data](#). See also policy information about [sex, gender \(identity/presentation\), and sexual orientation](#) and [race, ethnicity and racism](#).

Reporting on sex and gender

Previous experimental findings indicate sex differences in the response to brain insulin action affecting appetite, metabolism, and memory function. While increasing circulating estradiol and decreasing testosterone concentrations in healthy young men does not interfere with insulin's effect on food intake, the centrally mediated effect of insulin on peripheral insulin sensitivity in females critically depends on their menstrual cycle phase. Since this is the first study investigating the temporal dynamics of brain insulin action in response to an unhealthy diet, we only evaluated brain insulin action in response to overeating in normal-weight male participants. Whether the findings can be extended to females needs to be investigated in future studies.

Reporting on race, ethnicity, or other socially relevant groupings

Participants with high levels of education and a high socio-economic status are enriched in this study population. Given the repeated measurement design and the inclusion of a control group, we do not expect an impact on the results.

Population characteristics

29 male participants were aged 19 to 27 years, normal-weight (BMI range 19 – 25 kg/m²), nonsmokers, weight-stable for at least 3 months before the study visits, nondieters, no vegan or vegetarian dieters, no food allergies, exercising less than 2h a week, not working at night, not taking medication, and with no history of diabetes, eating disorders, illicit drug use, or other medical diagnoses. Gender was determined based on self-report and supported by testosterone measurements.

Recruitment

Participants were recruited by University-wide email announcements. Participants were not aware at the start of the study, if they were assigned to HCD or control group. As only young students were recruited, there was a selection bias towards high level of education but low income. This could be a selection bias. We do not expect this to impact our results, as both control and HCD group did not differ in this regard. Furthermore, the repeated measurement design minimize the impact of this bias.

Ethics oversight

Participants provided written informed consent in compliance with the University of Tübingen ethical committee. The study (813/2017BO2) received approval by the local ethics committee in January 2018 (Ethics Committee of the Medical Faculty of the Eberhard Karls University and the University Hospital Tübingen) and was conducted according to the relevant guidelines and regulations. The study is basic experimental study involving humans (BESH) and was registered at ClinicalTrials.gov (NCT03590561). A compensation of €600 was provided after completion of the study (total of 23 hours over 6 visits).

Note that full information on the approval of the study protocol must also be provided in the manuscript.

Field-specific reporting

Please select the one below that is the best fit for your research. If you are not sure, read the appropriate sections before making your selection.

Life sciences Behavioural & social sciences Ecological, evolutionary & environmental sciences

For a reference copy of the document with all sections, see nature.com/documents/nr-reporting-summary-flat.pdf

Life sciences study design

All studies must disclose on these points even when the disclosure is negative.

Sample size

A previous study investigating brain insulin action (Kullmann et al 2015 Diab Care), showed a large effect size of Cohen's d greater than 1 could be achieved with 18 subjects per group to detect obesity-associated insulin resistance. Assuming a 2-sided t-test of, $\alpha=0.05$ and 80% power, a total sample size of at least 25 persons was calculated. To compensate for potential drop outs, n=7 were additionally recruited.

Data exclusions

We miss one fMRI measurement timepoint of the second follow up from N=1. This is presented in the supplementary file (consort file)

Replication

We confirm that the regions identified to be responsive to intranasal insulin in the current study we found in previous fMRI studies (by our and other groups) Ref: Kullmann et al Lancet D&E 2020; Nijssen et al 2023 Neuroendocrinology)

Randomization

The allocation of the groups was not randomized as the experimental group received instructions by a nutritional scientist how to increase their caloric content, while the control group received instructions how to maintain their regular diet.

Blinding

Persons performing fMRI data acquisition and fMRI data analysis were blinded to experimental groups.

Reporting for specific materials, systems and methods

We require information from authors about some types of materials, experimental systems and methods used in many studies. Here, indicate whether each material, system or method listed is relevant to your study. If you are not sure if a list item applies to your research, read the appropriate section before selecting a response.

Materials & experimental systems

- n/a Involved in the study
- Antibodies
- Eukaryotic cell lines
- Palaeontology and archaeology
- Animals and other organisms
- Clinical data
- Dual use research of concern
- Plants

Methods

- n/a Involved in the study
- ChIP-seq
- Flow cytometry
- MRI-based neuroimaging

Clinical data

Policy information about [clinical studies](#)

All manuscripts should comply with the ICMJE [guidelines for publication of clinical research](#) and a completed [CONSORT checklist](#) must be included with all submissions.

- Clinical trial registration
- Study protocol
- Data collection
- Outcomes

Plants

- Seed stocks
- Novel plant genotypes
- Authentication

ChIP-seq

Data deposition

- Confirm that both raw and final processed data have been deposited in a public database such as [GEO](#).
- Confirm that you have deposited or provided access to graph files (e.g. BED files) for the called peaks.

- Data access links
- Files in database submission
- Genome browser session (e.g. [UCSC](#))

Methodology

- Replicates
- Sequencing depth
- Antibodies

Peak calling parameters	<i>Specify the command line program and parameters used for read mapping and peak calling, including the ChIP, control and index files used.</i>
Data quality	<i>Describe the methods used to ensure data quality in full detail, including how many peaks are at FDR 5% and above 5-fold enrichment.</i>
Software	<i>Describe the software used to collect and analyze the ChIP-seq data. For custom code that has been deposited into a community repository, provide accession details.</i>

Flow Cytometry

Plots

Confirm that:

- The axis labels state the marker and fluorochrome used (e.g. CD4-FITC).
- The axis scales are clearly visible. Include numbers along axes only for bottom left plot of group (a 'group' is an analysis of identical markers).
- All plots are contour plots with outliers or pseudocolor plots.
- A numerical value for number of cells or percentage (with statistics) is provided.

Methodology

Sample preparation	<i>Describe the sample preparation, detailing the biological source of the cells and any tissue processing steps used.</i>
Instrument	<i>Identify the instrument used for data collection, specifying make and model number.</i>
Software	<i>Describe the software used to collect and analyze the flow cytometry data. For custom code that has been deposited into a community repository, provide accession details.</i>
Cell population abundance	<i>Describe the abundance of the relevant cell populations within post-sort fractions, providing details on the purity of the samples and how it was determined.</i>
Gating strategy	<i>Describe the gating strategy used for all relevant experiments, specifying the preliminary FSC/SSC gates of the starting cell population, indicating where boundaries between "positive" and "negative" staining cell populations are defined.</i>

Tick this box to confirm that a figure exemplifying the gating strategy is provided in the Supplementary Information.

Magnetic resonance imaging

Experimental design

Design type	Resting state
Design specifications	Resting-state cerebral blood flow measurements before and 30 min after intranasal insulin.
Behavioral performance measures	During MRI no behavior was assessed.

Acquisition

Imaging type(s)	Functional and Diffusion
Field strength	3 Tesla
Sequence & imaging parameters	Arterial spin labeling (PASL) images were obtained with a PICORE-Q2TIPS (proximal inversion with control for off-resonance effects (quantitative imaging of perfusion by using a single subtraction) sequence by using a frequency offset corrected inversion pulse and echo planar imaging readout for acquisition. In addition, high-resolution T1-weighted anatomical images were obtained. Diffusion-weighted images (DWIs) were acquired using an echo planar imaging sequence with 35 directions and GRAPPA acceleration factor 2.
Area of acquisition	Whole-brain
Diffusion MRI	<input checked="" type="checkbox"/> Used <input type="checkbox"/> Not used

Parameters An echo planar imaging sequence (70 axial slices, FOV = 220 mm², slice thickness = 2mm, TE = 54 ms, TR = 6500 ms) with 35 directions (b = 1000 s/mm²) and GRAPPA acceleration factor 2 was acquired. Moreover, eleven interspersed nondiffusion weighted volumes (b₀) were recorded. To improve SNR two averages were performed.

Preprocessing

Preprocessing software	Image preprocessing was performed using the ASLtbx with SPM12 (Wellcome Trust Centre for Neuroimaging). Functional images were motion corrected, coregistered to the individual anatomical image, and smoothed (full width half maximum: 6 mm). For Diffusion MRI, standard preprocessing and statistical analyses were performed using FMRIB (Functional Magnetic Resonance Imaging of the Brains's, Oxford University, UK) Software Library (FSL version 6.0).
Normalization	The high resolution T1-weighted image was normalized in Montreal Neurological Institute space (1 x 1 x 1 mm) using SPM12's unified segmentation normalization, and the resulting parameter file was used with the individual coregistered CBF maps in normalized space (3 x 3 x 3 mm).
Normalization template	normalized in Montreal Neurological Institute (MNI305)
Noise and artifact removal	Six head motion parameters. No participant had head motion with more than 2.0 mm maximum displacement or 2.0° of any angular motion.
Volume censoring	NA

Statistical modeling & inference

Model type and settings	For functional MRI, perfusion images were generated by calculating the control-tag differences by using surround subtraction. For accurate CBF quantification ($\text{ml} \times 100\text{g}^{-1} \times \text{min}^{-1}$), we used unique M0 value extracted from a ROI in the cerebro spinal fluid. We used the general kinetic model for absolute perfusion quantification. The absolute change of CBF of each participant from before to after intranasal insulin spray application were used for further statistics ($\Delta\text{CBF} = \text{CBF 30 min post nasal spray} - \text{CBF before nasal spray}$).
Effect(s) tested	Flexible factorial design (to investigate group differences, while taking into account within subject variability)
Specify type of analysis:	<input checked="" type="checkbox"/> Whole brain <input type="checkbox"/> ROI-based <input type="checkbox"/> Both
Statistic type for inference	Whole-brain analyses were performed using a voxel-wise approach in SPM12
(See Eklund et al. 2016)	
Correction	For functional data: A statistical threshold of $p < 0.001$ uncorrected and a $p < 0.05$ family wise error (FWE) corrected for multiple comparisons was applied on a whole brain level. For tract-based spatial statistics, we used the module randomise in FSL. It is a non-parametric permutation test for inference on statistical maps. For detecting significant clusters corrected for multiple comparisons, we selected the TFCE (Threshold-Free Cluster Enhancement) method optimized for TBSS analyses. Statistical maps were thresholded at $p < 0.05$ (TFCE corrected). The number of permutations was set to 5000.

Models & analysis

n/a	Involvement in the study
<input checked="" type="checkbox"/>	<input type="checkbox"/> Functional and/or effective connectivity
<input checked="" type="checkbox"/>	<input type="checkbox"/> Graph analysis
<input checked="" type="checkbox"/>	<input type="checkbox"/> Multivariate modeling or predictive analysis